# Bioinspired Capillary Force-Driven Super-Adhesive Filter

Junyong Park[1], Chan Sik Moon[1], Ji Min Lee[1], Sazzadul A. Rahat[2], Sang Moon Kim[3], Jonathan T. Pham[2,4], Michael Kappl[5], Hans-Jürgen Butt[5], and Sanghyuk Wooh[1]*

[1]*Department of Chemical Engineering, Chung-Ang University, Seoul, 06974, Republic of Korea*

[2]*Department of Mechanical and Materials Engineering, University of Cincinnati, Ohio, 45221, USA*

[3]*Department of Mechanical Engineering, Incheon National University, Incheon, 22012, Republic of Korea*

[4]*Department of Chemical and Environmental Engineering, University of Cincinnati, Ohio, 45221, USA*

[5]*Max Planck Institute for Polymer Research, Mainz, 55128, Germany*

**Keywords**

: Adhesion, air filter, capillary force, surface modification, thin liquid film.

***Equal contribution**

: Junyong Park and Chan Sik Moon

*Corresponding author. Email: woohsh@cau.ac.kr

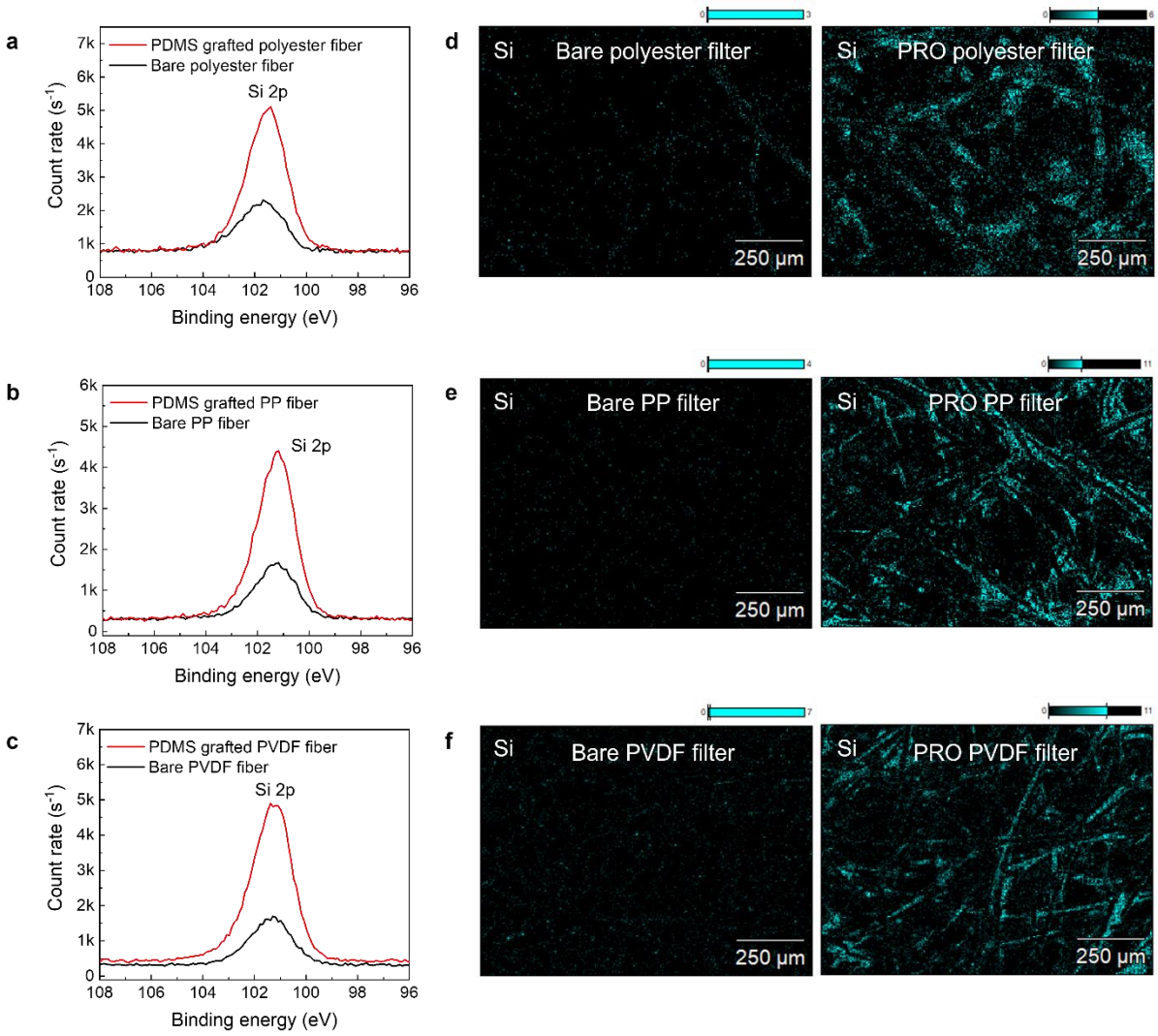


**Figure S1. Elemental characterization. a-c**, XPS spectra indicating Si 2p element on the surface of bare (black line) and PDMS grafted (red line) (**a**) polyester, (**b**) PP, and (**c**) PVDF filter fiber. **d-f**, EDS analysis images representing Si of (**d**) polyester, (**e**) PP, and (**f**) PVDF filters. Left and right are bare and PRO filters, respectively.

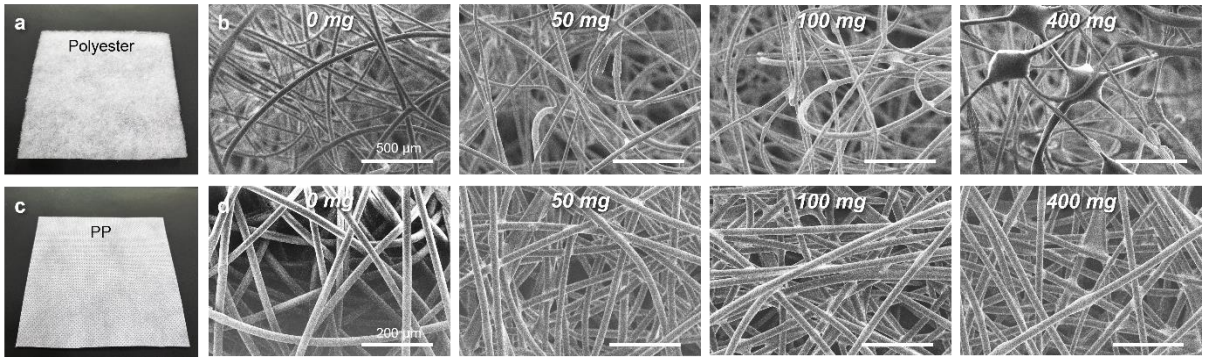


**Figure S2. Characterization of pore structures of the PRO filters.** Photographs of (**a**) polyester and (**c**) polypropylene (PP) non-woven filters, and SEM images of (**b**) polyester and (**d**) PP non-woven filters including different amounts of silicone oil. 0 mg samples indicate bare filters. For the PRO filters, 50 mg, 100 mg, and 400 mg silicone oil were deposited on the filter media with a unit area of 100 $cm^2$.

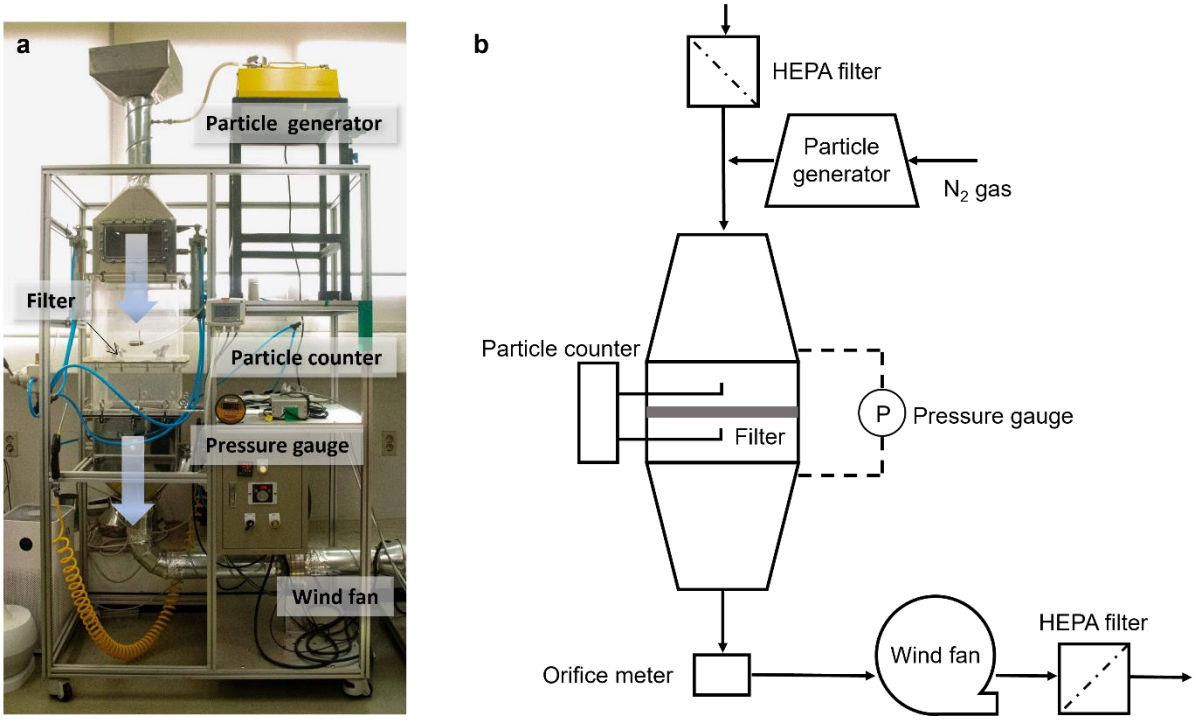


**Figure S3. Filtering performance testing chamber.** (**a**) A photograph and (**b**) a schematic design of a custom-built filtering performance testing chamber. The chamber is designed by following the filtration performance measurement standard, DIN 71460-1:2006.

KITECH
Korea Institute of Industrial Technology
89, Yangdaegiro-gil, Ipjang-myeon, Seobuk-gu, Cheonan-si,
Chungcheongnam-do 31056 Republic of Korea
Tel: +82-41-589-8114 | Fax: +82-41-589-8120
www.kitech.re.kr

1. Certificate No. : C21N230722-02
2. Client Name : Chung-Ang University's Industry-Academic Cooperation Foundation
3. Sample name : Polyester Bare I / 305×220×7 $mm^3$
4. Test method used : DIN 71460-1:2006
   - Flow rate: 500 $m^3/h$
   - Test dust: ISO A2 Fine dust
   - Dust concentration: 20 $mg/m^3$
5. Test results :

○ Test results

| Particle size (μm) | Initial fractional efficiency (%) |
|---|---|
| 0.3 ~ 1.0 | 14.1 |
| 1.0 ~ 2.5 | 59.8 |
| 2.5 ~ 10.0 | 66.2 |

○ Test sample

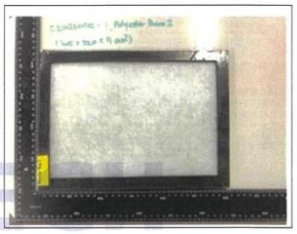

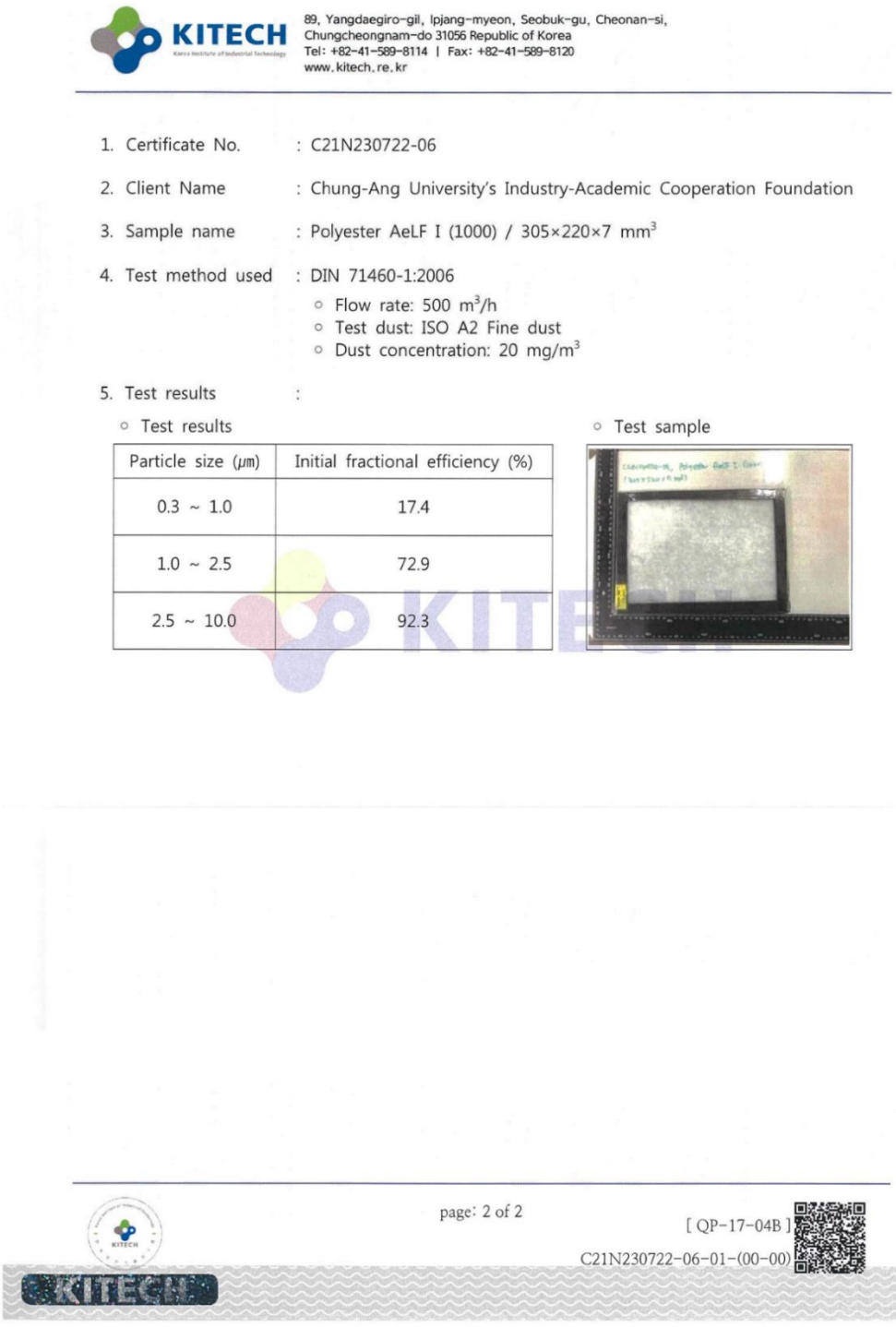

KITECH
89, Yangdaegiro-gil, Ipjang-myeon, Seobuk-gu, Cheonan-si,
Chungcheongnam-do 31056 Republic of Korea
Tel: +82-41-589-8114 | Fax: +82-41-589-8120
www.kitech.re.kr

1. Certificate No. : C21N230722-06
2. Client Name : Chung-Ang University's Industry-Academic Cooperation Foundation
3. Sample name : Polyester AeLF I (1000) / 305×220×7 $mm^3$
4. Test method used : DIN 71460-1:2006
   - Flow rate: 500 $m^3/h$
   - Test dust: ISO A2 Fine dust
   - Dust concentration: 20 $mg/m^3$
5. Test results :

- Test results

| Particle size (μm) | Initial fractional efficiency (%) |
|---|---|
| 0.3 ~ 1.0 | 17.4 |
| 1.0 ~ 2.5 | 72.9 |
| 2.5 ~ 10.0 | 92.3 |

- Test sample

page: 2 of 2
[ QP-17-04B ]
C21N230722-06-01-(00-00)

**Figure S4. Filtration efficiency reports by authorized testing institution.** Filtration efficiency reports, tested by Korea Institute of Industrial Technology (KITECH), which is an authorized filtration testing institution. The test was carried out by following DIN 71460-1:2006 testing standard. Face velocity for the tests was approximately 2.8 m/s at a flow rate of 500 $m^3/h$.

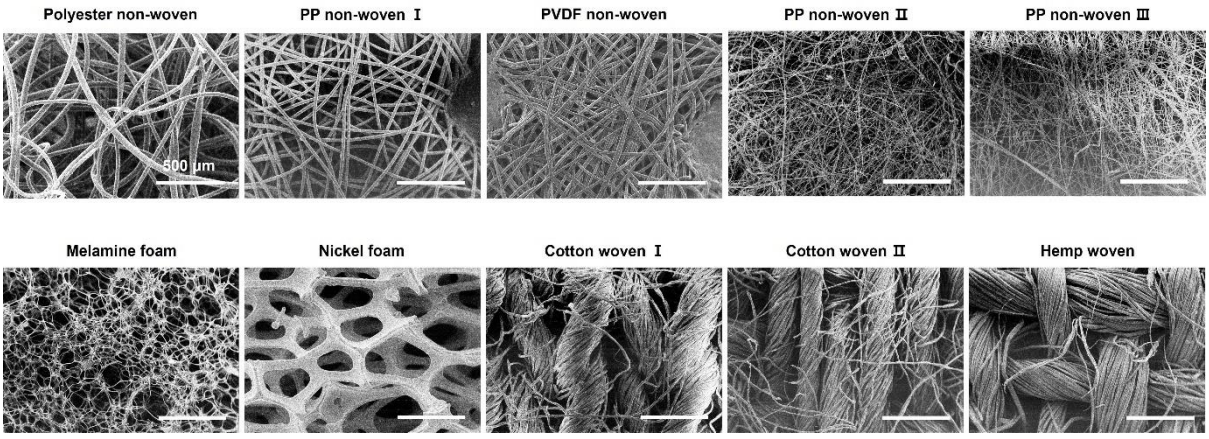


**Figure S5. SEM images of various filter media.** Morphologies of various filter media used for the FE characterizations, shown in Fig. 2a. Investigated filter material: polyester, PP, polyvinylidene fluoride (PVDF), melamine, nickel, cellulose.

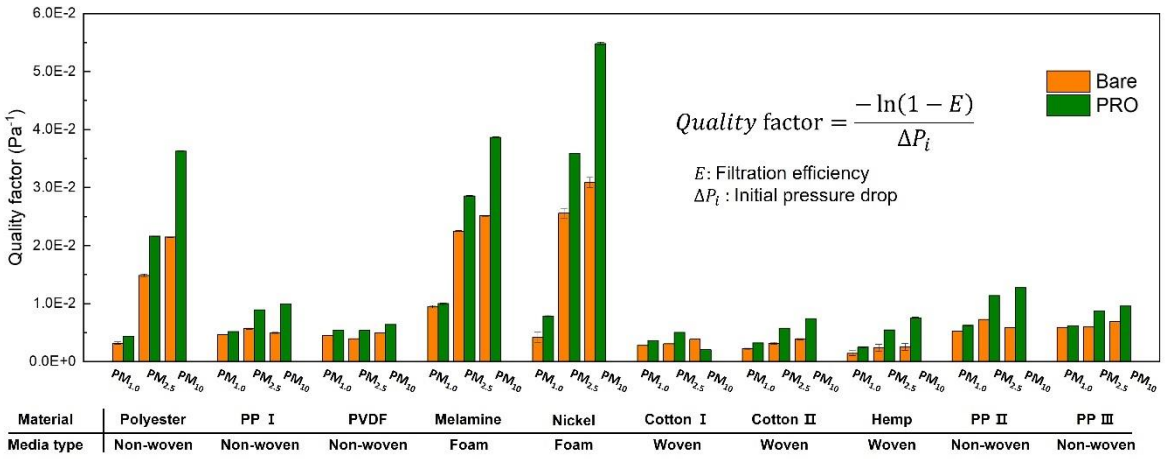


**Figure S6. Quality factors of filters.** Quality factors of filters in Fig. 2a, which were calculated by using FEs and *Δ*P. The equation inside represents the definition of the quality factor that provides a comprehensive index of filtering performance, considering FE and the associated *Δ*P across the filter.

Section 1: Effect of Viscosity of Silicone Oil on Filtration Performance

We tested the influence of viscosity of silicone oil on filtration performance by testing with silicone oils of different viscosities—100, 1000, 5000, and 10000 cSt—in identical amount. A polyester filter (air permeability: 325.6 ± 4.0 $cm^3/s/cm^2$) and a PP filter (134.8 ± 1.9 $cm^3/s/cm^2$) were used to investigate the effect of viscosity of silicone oil on filtration performances. In fact, capillary force is independent to viscosity of oil as depicted in fig. S10. The experimental results, shown in fig. S7, confirms that FEs also rarely influenced by viscosity of oil due to the similar adhesion by capillary force.

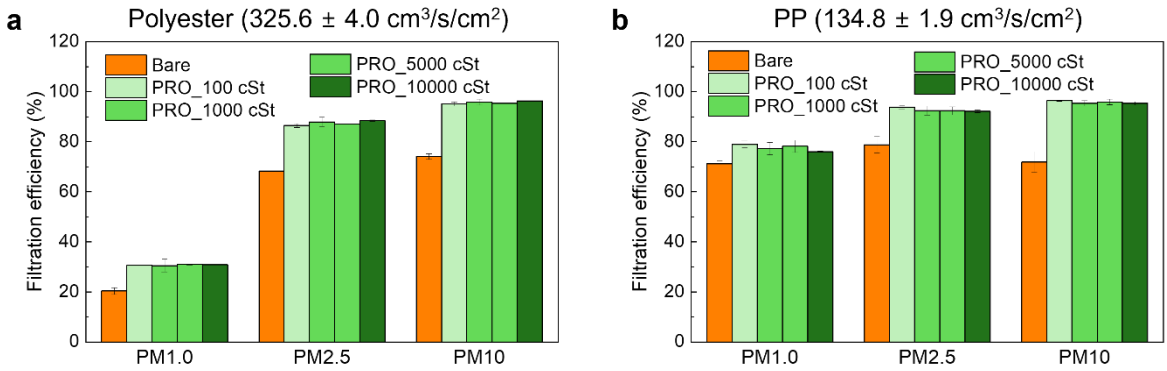


**Figure S7. Filtration performances with varied viscosities of silicone oil.** FEs of (**a**) polyester and (**b**) PP filters as a function of viscosity of silicone oil, ranging from 100 to 10000 cSt.

Section 2: Stability of Thin Silicone Oil Layer

Non-volatile silicone oil integrated with PDMS brush-grafted surface was known to generate long-term stable thin liquid layer[14,15]. To investigate the stability of silicone oil layer on filter media, we first examine the FEs of the 16 months stored PRO filter, as shown in fig. S8. The PRO filter was stored in a dust-blocked chamber to minimize efficiency change caused by airborne particle adsorption. After the 16 months of storage, filtration performance test was performed. The FEs of the 16 months stored PRO filter exhibited almost identical FEs of the fresh PRO filter, confirming the long-term stable oil layer.

Under airflow, the oil layer is more unstable and can be detached from the substrate if the oil layer is thick and inhomogeneous[44-46]. Therefore, we tested a stability of silicone oil by using particle counter at the filtering test chamber without applying PM. The test was performed under airflow of 2 m/s. The number of particles behind the bare and PRO filter were nearly the same. In fact, it is the particles existing in the chamber; similar number of particles are detected even without any filter. The results, shown in fig. S9, verifies no silicone oil detachment under rapid airflow.

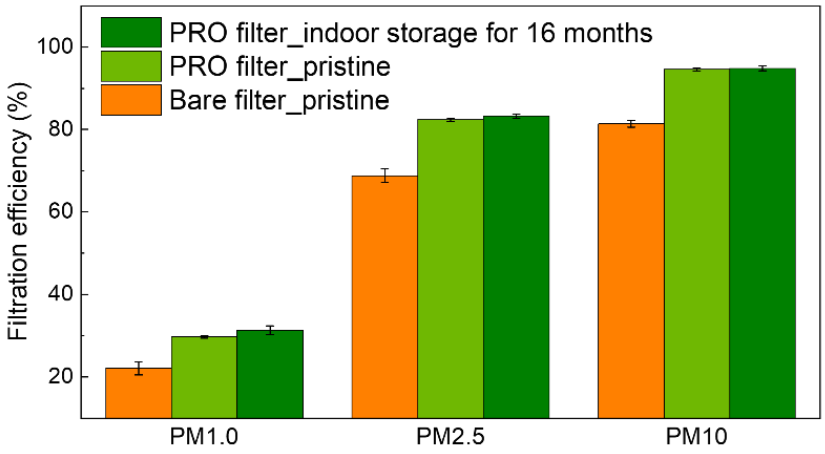


**Figure S8. Long-term stability of PRO filter.** FEs of bare, fresh-made PRO filter, and 16 months stored PRO filter. Polyester filter was used as the filter media.

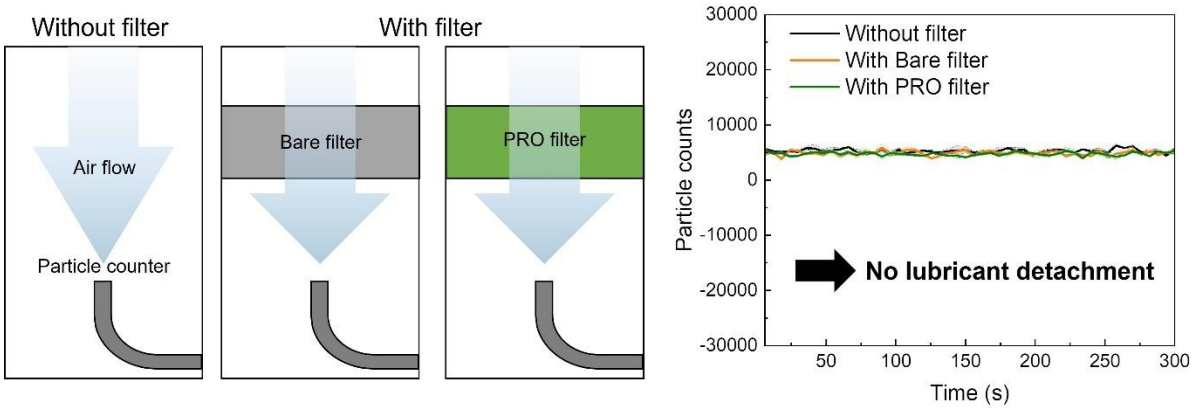


**Figure S9. Stability test under airflow.** Illustrations elucidating liquid layer stability testing experiment using particle counter under airflow without PM deposition. Line with shaded area indicating average counts of particle with error. Particle counts without filter, drawn with black line, indicates ever-present airborne particles in the chamber.

Section 3: Calculation of Particle Adhesion and Drag Forces

We conducted a theoretical investigation to understand the correlation between enhanced FE and adhesion force. This was based on experimental data and accounted for particle trapping mechanisms. Specifically, particles making contact with the filter surface would be more effectively retained if the adhesion force between the particles and filter fiber were elevated. To quantify this, we calculated the adhesion forces for each case. For a bare solid filter, the adhesion force was calculated based on the van der Waals force ($F_{vdw}$), since the interface in this case is characterized by solid-solid contact. The van der Waals force is expressed as[39]:

$$F_{vdw} = \frac{Ad}{12z_0^2} \quad (1)$$

where $d$ is the particle diameter, $z_0$ is the effective distance between surfaces, $A$ is Hamaker's constant. Silicone oil coated on PRO substrate forms a solid-liquid interface with the particles and exerts a capillarity on the attached particles. Capillary force ($F_c$) is expressed as follows[35]:

$$F_c = \pi \cdot d \cdot \gamma \cdot sin\,\beta \cdot sin\,(\beta + \theta) \quad (2)$$

where $\gamma$ denotes the surface tension of the liquid, $\theta$ represents the contact angle, and $\beta$ denotes the filling angle indicating three-phase contact angle on the particle surface.

Initially, we validated the alignment of these theoretical considerations with empirical observations. For solid-solid interfaces, we measured the adhesion forces between a bare glass substrate and both silica and polyethylene beads. The effective separation distance was inferred from the force-distance curve depicted in Extended Data Fig. 5. The Hamaker constant, calculated based on these adhesion force measurements, fell within the expected range of $6\times10^{-20}$ to $150\times10^{-20}$ J, validating that the experimental outcomes for solid-solid interfaces are congruent with theoretical expectations[39].

To compute the capillary forces generated by the meniscus, values for each $\theta$ and $\beta$ of the silicone oil meniscus around the bead were required. We utilized confocal microscope to obtain cross-

sectional image of the meniscus and measure the contact angles. Even though the larger particle than particle used in the adhesion analysis was used due to the resolution constraints of confocal microscope, we postulated that the meniscus would exhibit a similar shape irrespective of particle size in an equilibrium state. Based on fig. S10, the silicone oil meniscus exhibited a contact angle $\theta$ of approximately 30° and a filling angle $\beta$ of approximately 90°. The surface tension for silicone oil was taken as 21 mN/m. Subsequently, we verified that the experimentally measured adhesion force induced by silicone oil on silica and polyethylene beads corresponded to the theoretical calculations within acceptable limits.

Notable merit of the PRO filter lies in its ability to sustain FE even at elevated face velocities exceeding 2.5 m/s, a condition under which the bare solid filter experiences efficiency degradation. This decrease in efficiency for the bare solid filter can be ascribed to the removal of previously adhered particles from the filter surface due to the drag force of fluid. Therefore, the interplay between this drag force and the adhesion force acting on the particles governs the contrasting performances of the PRO and bare solid filters. As the adhesion force specific to each filter has already been examined, it becomes imperative to consider the drag force exerted on adhered particles to comprehensively understand this force balance. The drag force induced by fluid flow is formulated as follows[39]:

$$F_{drag} = C_D \frac{\pi}{8} \rho_g d^2 V^2 \tag{3}$$

where $\rho_g$ is the fluid density, $V$ is the fluid velocity, and $C_D$ is the drag coefficient. And $C_D$ is differently determined with a dependence of Reynolds number ($Re = \rho_g V d/\mu$; $\mu$ is viscosity of fluid) as expressed as:

$C_D = \frac{24}{Re}$ for $Re \leq 1$ : Stokes' law region

$C_D = \frac{24}{Re}(1 + 0.15Re^{0.687})$ for $1 < Re \leq 1000$ : Transition region

$C_D \approx 0.44$ for $Re > 1000$ : Newton's law region

Given that the working fluid is air, characterized by a density of 1.20 kg/m$^3$ and viscosity of $1.81\times10^{-5}$ N·s/m$^2$, the Reynolds number is expected to fall within either the Stokes' law region or the transition region under these experimental conditions. The drag force, when adhering to Stokes' law, is formulated as follows:

$$F_{drag,stoke} = \frac{24}{Re}\frac{\pi}{8}\rho_g d^2V^2 = \frac{24\mu}{\rho_g V d}\frac{\pi}{8}\rho_g d^2V^2 = 3\pi\mu dV \quad (4)$$

In the transition region, the drag force is calculated according to the following equation:

$$F_{drag,trans} = \frac{24}{Re}(1 + 0.15Re^{0.687})\ \frac{\pi}{8}\rho_g d^2V^2 \quad (5)$$

If the magnitude of the drag force exceeds that of the adhesion force, particles previously adhered to the surface will detach, resulting in a decline in FE. Prior to analyzing this force equilibrium, it is necessary to investigate the medium velocity that particles experience due to the porous nature of the media. This medium velocity ($V_m$) is related to the face velocity ($V_f$) as follows[47]:

$$V_m = \frac{V_f}{(1-p)} \quad (6)$$

where $p$ is the medium packing density. The polyester filter employed in this study exhibited a porosity of approximately 90%, resulting in an estimated $p$ value of approximately 10%. Consequently, the face velocity corresponding to a Reynolds number of 1—which serves as the demarcation between the Stokes' law region and the transition region—can be calculated for each particle size. We defined $PM_{1.0\mu m}$ as particle sized only 1.0 μm in diameter. According to Extended Data Fig. 6b, the velocities were determined to be 13.6 m/s for $PM_{1.0\mu m}$, 5.5 m/s for $PM_{2.5\mu m}$, and 1.4 m/s for $PM_{10\mu m}$. These findings indicate that $PM_{1.0\mu m}$ and $PM_{2.5\mu m}$ cases fall within the Stokes' law region, while the $PM_{10\mu m}$ case resides in the transition region, given that the maximum face velocity in the experiments was 4 m/s. Subsequent to these observations, the critical medium velocity ($V_{cr}$) was computed for each scenario, taking into account the balance between drag and adhesion forces. Should the medium velocity surpass this critical threshold, particles that had been adhered to the

surface would detach, leading to a decline in filtration efficacy. Within the Stokes' law region for a bare solid filter, the critical velocity, denoted $V_{(cr,Stokes,solid)}$, can be obtained using the following equation:

$$F_{vdw} = \frac{Ad}{12z_0^2} = F_{drag,Stokes} = 3\pi\mu d V_{(cr,Stokes,solid)} \quad (7\text{-}1)$$

$$V_{(cr,Stokes,solid)} = \frac{A}{36\pi\mu z_0^2} \quad (7\text{-}2)$$

Remarkably, the critical velocity under Stokes' law is independent of particle size. The computed values for the critical media and face velocities were 3.26 m/s and 2.9 m/s, respectively, in the case of a bare solid filter. Considering that the efficiency of the bare solid filter begins to decline at a face velocity of 2.4 m/s for $PM_{2.5\mu m}$, this is in close agreement with the critical face velocity of 2.9 m/s. For the transition region, the balance between the drag force and the adhesion force is assessed as follows:

$$F_{vdw} = \frac{Ad}{12z_0^2} = F_{drag,trans} = \frac{24}{Re}(1 + 0.15Re^{0.687})\ \frac{\pi}{8}\rho_g d^2 V_{(cr,trans,solid)}^2 \quad (8\text{-}1)$$

$$V_{(cr,trans,solid)} = \left(\frac{A}{36\pi\rho_g z_0^2 d}\frac{Re}{(1+0.15Re^{0.687})}\right)^{1/2} \quad (8\text{-}2)$$

Extended Data Fig. 6c presents a plot of $V_{(cr,solid)}$, a composite of the critical velocities in both the Stokes and transition regions, as functions of the face velocity and particle size, along with $V_m$ as a function of $V_f$. When $V_m$ exceeds $V_{(cr,solid)}$ there exists a substantial likelihood of observing a decline in filtration efficiency due to elevated drag forces. The theoretical critical face velocity for $PM_{10\mu m}$ was estimated to be 2.4 m/s. Although the empirical filtration efficiency for $PM_{10\mu m}$ began to decrease from the outset, diverging from the theoretical value, the observation is still valuable.

In contrast to the performance decline observed in the bare solid filter at elevated fluid velocities, the PRO filter exhibited efficiency sustainment, even at face velocities as high as 4 m/s. To

account for this, we applied the same theoretical framework, replacing the $F_{vdw}$ with the $F_c$ in our calculations.

$$F_c = \pi d\gamma sin\,\beta sin\,(\beta+\theta) = F_{drag,Stokes} = 3\pi\mu d V_{(cr,Stokes,liquid)} \quad (9\text{-}1)$$

$$V_{(cr,Stokes,liquid)} = \frac{\gamma \sin\beta \sin(\beta+\theta)}{3\mu} \quad (9\text{-}2)$$

$$F_c = \pi d\gamma sin\,\beta sin\,(\beta+\theta) = F_{drag,trans} = \frac{24}{Re}(1+0.15Re^{0.687})\,\frac{\pi}{8}\rho_g d^2 V^2_{(cr,trans,liquid)} \quad (10\text{-}1)$$

$$V_{(cr,trans,liquid)} = \left(\frac{8\gamma sin\,\beta sin\,(\beta+\theta)}{\frac{24}{Re}(1+0.15Re^{0.687})\rho_g d}\right)^{1/2} \quad (10\text{-}2)$$

The critical velocities for the PRO filter, plotted against face velocity, are displayed in Extended Data Fig. 6d. The data indicates critical velocities of 158.9 m/s for $PM_{1.0\mu m}$, 125.3 m/s for $PM_{2.5\mu m}$, and 82.0 m/s for $PM_{10\mu m}$. These velocities are markedly higher than those for the bare solid filter, substantiating the notion that the PRO filter is capable of exceptional filtration performance even under demanding conditions. These theoretical analyses validate the superior efficacy of the PRO filter, attributable to augmented adhesion forces.

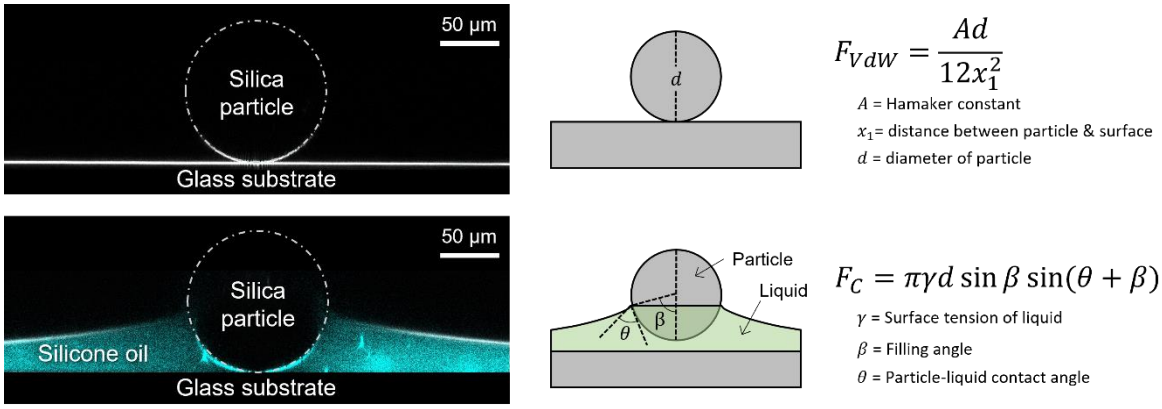


**Figure S10. Particle adhesions on solid and thin liquid layer coated substrates.** Confocal microscope images of silica particle adhered to uncoated (left top) and oil-coated (left bottom) glasses. The right schematics represent theoretical adhesion forces applying to each substrate.

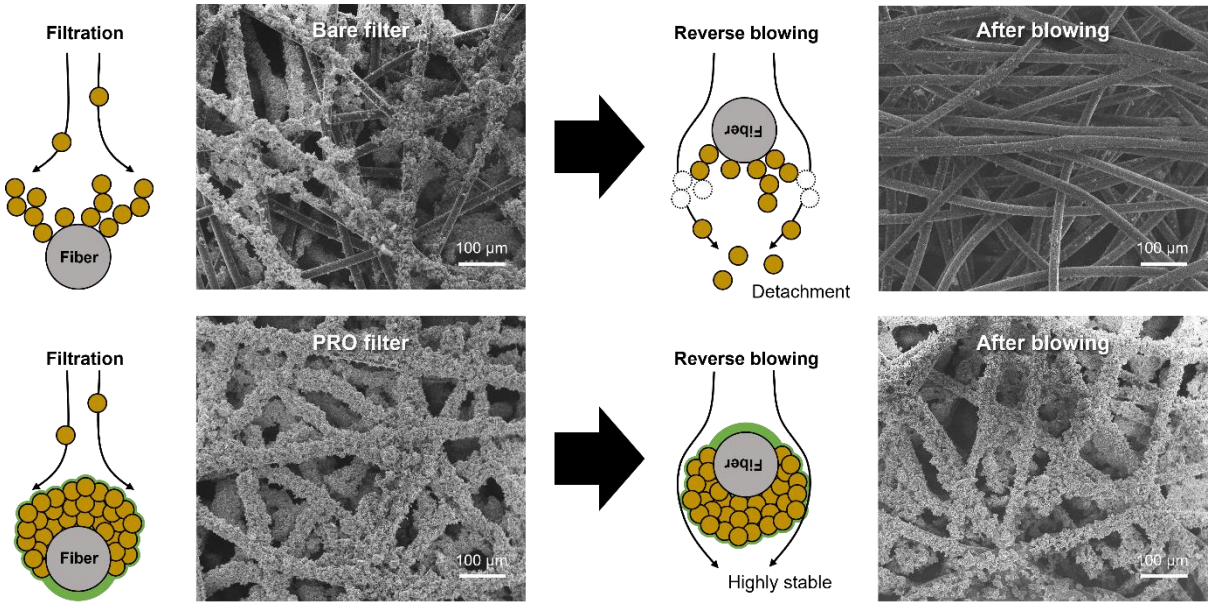


**Figure S11. PM adhesion properties during resuspension test.** Schematics of resuspension test and SEM images of bare (top) and PRO (bottom) filter before and after the reverse air blowing.

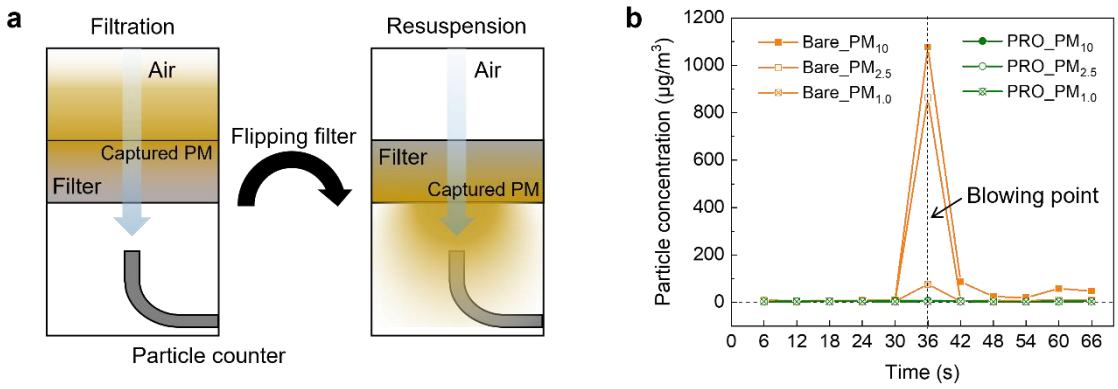


**Figure S12. Quantitative analysis of PM detachment**. **a**, Schematic of the testing procedure to quantify the PM detachment in the filtration testing chamber. After depositing the PM onto the filter (left), the PM captured filter was inverted, exposing clean airflow from the backside (right), then PM concentration behind the filter was measured by particle counter. **b**, Changes in PM concentrations behind the filters when clean air is blown. The concentrations were measured every 6 seconds.

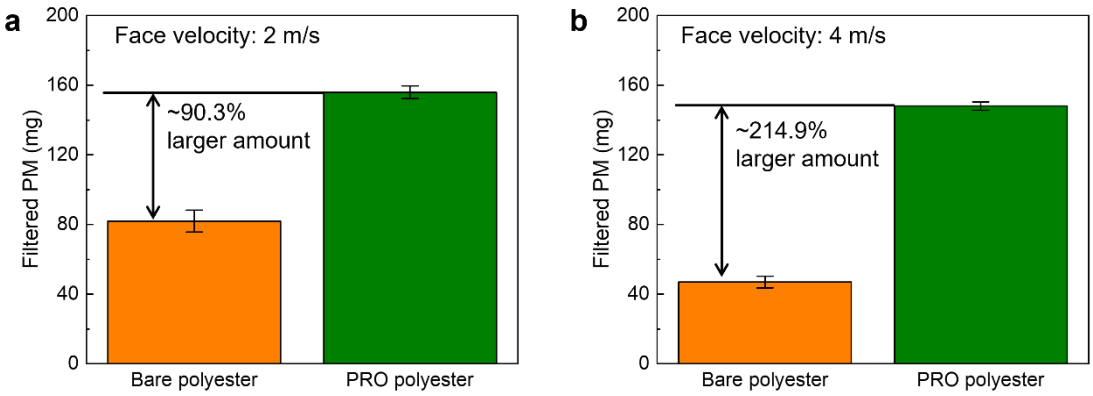


**Figure S13. Weight of captured PM on filters.** Filtered PM weight at face velocities of (**a**) 2 m/s and (**b**) 4 m/s. Total weight of filtered PM was determined by comparing weight of before and after filtration, with approximately 180 mg of PM applied in each test.

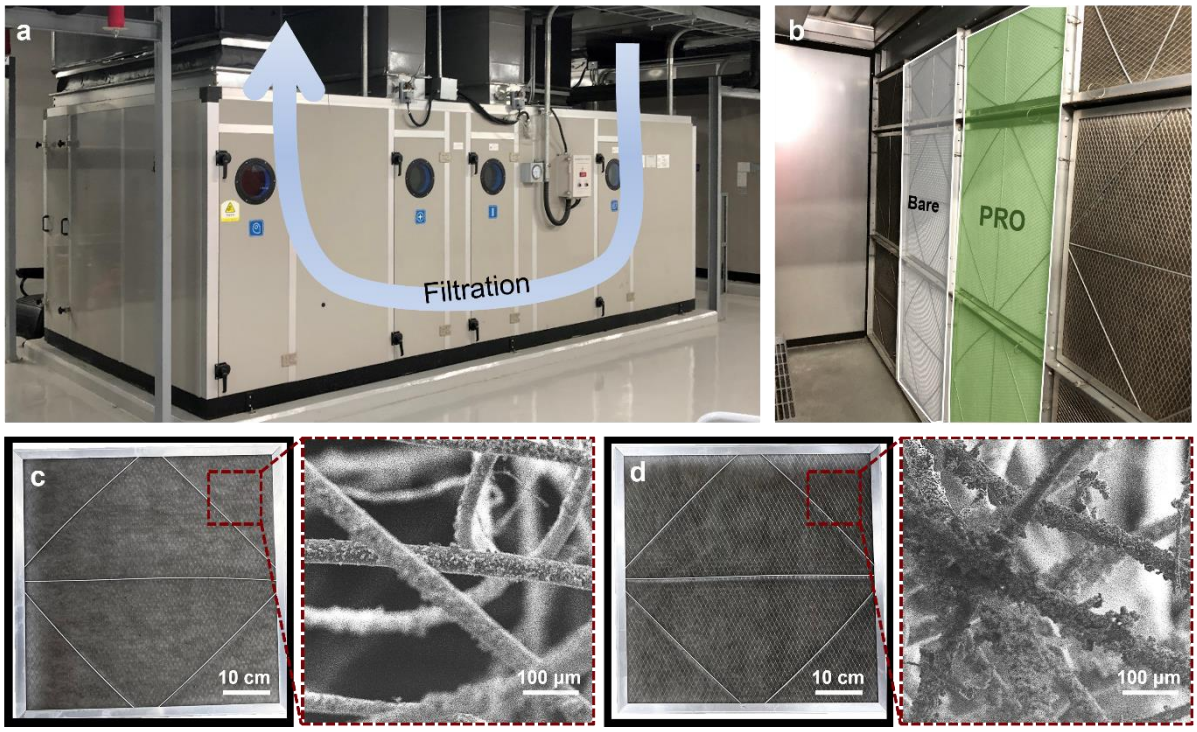


**Figure S14. Empirical validation of filter efficacy. a**, Outside view of the heating, ventilation, and air conditioning (HVAC) system in an air-conditioning room, located at the building 310 of Chung-Ang University, Seoul Campus. **b**, Inside view of the HVAC system with the bare (white box) and the PRO (green box) filters. Photos (left) and SEM images (right) of (**c**) the bare and (**d**) the PRO pre-filters after 3 months of operation.

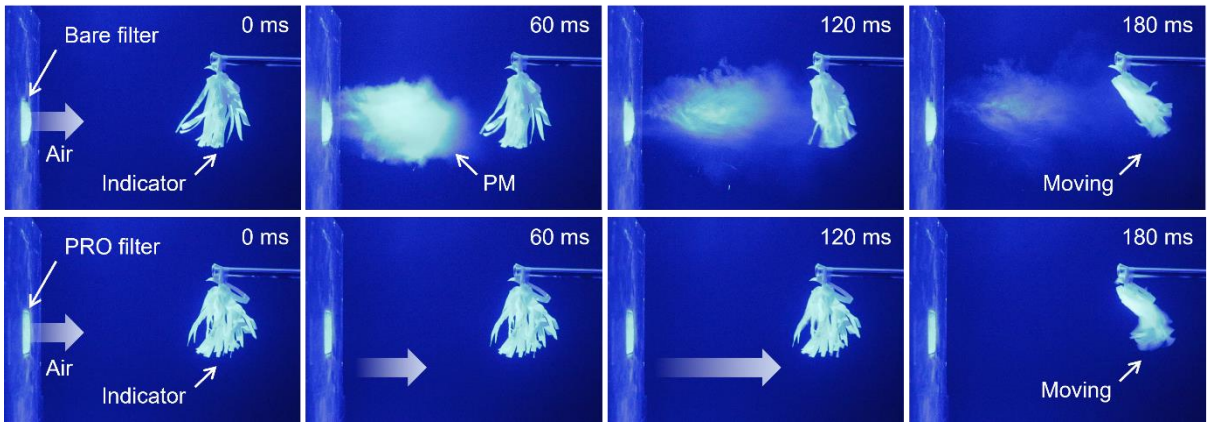


**Figure S15. Visualization of PM resuspension.** Snapshot images of air blowing through the bare (top) and the PRO (bottom) filters. Before the air blowing, similar amount of PM was deposited to both filters. The images were taken at the blue light chamber that can clearly show a cloud of PM dispersed from the filter.

Section 4: Reusability of PRO Filters

Following the filtration process, PRO filters can be regenerated by washing. The reusability test of the PRO filter was conducted by washing and recoating process. It was demonstrated by using PP based pre- and HEPA filter. The thin silicone oil layer can be washed with detergent water or hexane, thereby removing captured PMs. The PRO pre-filter can easily be washed by shaking the filter in a detergent water. More vigorous washing in hexane is required to wash the HEPA filter due to its small pores. After the washing step, the filters were dried, and the thin oil layer was regenerated by coating the silicone oil. Subsequent reformation of the thin silicone oil layer restores the initial filtration performance of the PRO filter. We found that this regeneration process can be repeated more than five times without degrading the filtration efficacy, leading to a significant reduction in filter waste (Fig. S16).

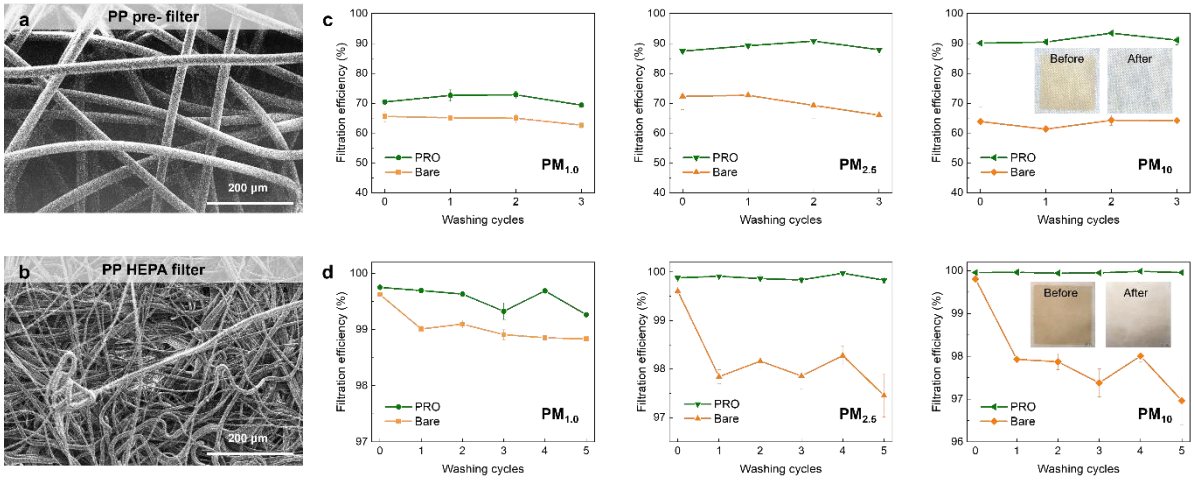


**Figure S16. Reusability test.** SEM images of PP (**a**) pre- and (**b**) HEPA filter. FEs of PP (**c**) pre- and (**d**) HEPA filter representing as a function of washing cycles. Images of filters in filtration efficiency of $PM_{10}$ (the right graphs) additionally verifies removal of PM trapped on PP filters by washing with detergent water and/or hexane.

## Reference


44 Davoudi, M., Amrei, M. M., Tafreshi, H. V. & Chase, G. G. Measurement of inflection angle and correlation of shape factor of barrel-shaped droplets on horizontal fibers. *Sep. Purif. Technol.* **204**, 127-132, doi:https://doi.org/10.1016/j.seppur.2018.04.033 (2018).

45 Amrei, M. M., Venkateshan, D. G., D'Souza, N., Atulasimha, J. & Tafreshi, H. V. Novel approach to measuring the droplet detachment force from fibers. *Langmuir* **32**, 13333-13339, doi:10.1021/acs.langmuir.6b03198 (2016).

46 Farhan, N. M. & Vahedi Tafreshi, H. Universal expression for droplet–fiber detachment force. *J. Appl. Phys.* **124**, doi:10.1063/1.5032106 (2018).

47 Abdolghader, P., Brochot, C., Haghighat, F. & Bahloul, A. Airborne nanoparticles filtration performance of fibrous media: A review. *Sci. Technol. Built Environ.* **24**, 648-672, doi:10.1080/23744731.2018.1452454 (2018).